AIAA JOURNAL
Vol. 40, No. 4, April 2002

Assessment of the Accuracy of Representing a Helical Vortex by Straight Segments

D. H. Wood* and D. Li†
University of Newcastle, Callaghan, New South Wales 2308, Australia

The accuracy of representing a helical vortex, as found in the wakes of helicopters, wind turbines, and propellers, by a sequence of straight segments is considered. The accuracy is assessed by comparison with recent results for the induced velocity of a helix of constant pitch and radius. This comparison is motivated by the small values of the vortex pitch behind wind turbines and hovering rotors; small pitch leads to errors associated with the proximity of subsequent turns of the helix to the control point at which the velocity is required. Three cases are considered. The first, the velocity on the helix axis, has an analytic solution, which is used to demonstrate that the general accuracy of the straight segment approximation is second order, as has been found in previous comparisons with the velocity field of a vortex ring. For the second case, where the control point has the same radius as the vortex, the segments aligned with the control point are mainly responsible for the error. The error varies from first to third order as the number of segments per revolution of the helix is increased. Third, the self-induced velocity is determined to within an accuracy comparable with the effects of the vortex structure, of which little is presently known in general. The effects of vortex curvature are not significant and easily dealt with.

Nomenclature

a	=	vortex core radius
L	=	length of vortex segment
M	=	number of straight segments per revolution of the helix
N	=	number of helical vortices
p	=	vortex pitch
R	=	helix radius
r	=	distance
U	=	x direction velocity
U_b	=	binormal velocity
W	=	z direction velocity
$W(p)$	=	integral in Eq. (1); typical values in Table 1
$W(\alpha, p)$	=	integral in Eq. (1); typical values in Table 1
x, y, z	=	coordinate directions defined in Fig. 1
α	=	azimuthal displacement of vortex
Γ	=	circulation in vortex
Δ	=	error; Eq. (6)
ε	=	cutoff parameter
θ	=	vortex angle

Subscripts

a	=	start of vortex segment
b	=	end of vortex segment
p	=	control point
s	=	value for vortex segment

Introduction

IT is common for the helical vortices in the wakes of propellers, rotors, and wind turbines to be represented computationally by a sequence of straight vortex segments, e.g., Refs. 1–6. This approximation is shown schematically in Fig. 1 for one revolution of a helix of constant diameter and pitch. The number of segments per revolution is M, which will be treated as an integer; $M = 6$ in Fig. 1. The straight segment approximation is computationally simple and is easily incorporated into methods that iterate to achieve a free-wake geometry, e.g., Ref. 5. The accuracy of the approximation, however, has been tested thoroughly only for the known velocity field of a vortex ring, e.g., Refs. 2, 5, and 6. It is shown in those references that straight segments have an error proportional to M^{-2}. In other words, the approximation has the same order of accuracy as the trapezoidal rule applied to the original Biot–Savart integral. Testing has been limited to vortex rings partly because the velocity field of helical vortices is considerably more complex, even when the vortices are doubly infinite and have constant pitch and diameter.[7–10] It is only recently that the full expression for the self-induced velocity of a helical vortex has been found by Boersma and Wood.[11] Wood and Boersma[12] extended the analysis to include the motion of N identical vortices with a common axis, each azimuthally displaced by $2\pi/N$. This situation models the vortices trailing from an N-bladed rotor. Reference 12 considered $N = 2$, 3, and 4.

Testing against helices rather than rings is necessary because of the small values of the vortex pitch p in the wakes of rotors and wind turbines; Ref. 12 demonstrates that p, when normalized by R, as are all lengths in this paper, is typically about 0.05 for wind turbines operating at maximum efficiency, and Leishman et al.[13] measured $p = 0.053$ behind their hovering rotor. The helix in Fig. 1 has $p = 0.05$. The figure also shows the three test cases that will be considered: the control point for case 1 is on the centerline at the start of the vortex, for case 2 it shares the helix radius but is displaced axially by $p/2$ from the nearest point on the helix, and case 3 is the self-induced velocity. Figure 2 shows the integrand for the Biot–Savart law for case 2 for a range of p and for a vortex ring coinciding with the helix at $y = -1$. The vortex angle θ is measured from the positive y axis in Fig. 1 in the direction of the helix. For small p the rapid change in the integrand and the large maxima near $\theta = \pi$ in Fig. 2 will obviously cause problems for any numerical method. This behavior, which is repeated with diminishing significance every additional 2π, is caused by the proximity of the subsequent turns of the helix and does not occur for a vortex ring. In other words, the integrands in Fig. 2 emphasize that the vortex ring is not a special case of a helix at small p. The two peaks in the helix integrands are displaced from π by $\theta' \approx \pm\sqrt{(2)\pi p}$. It is reasonable, therefore, to require that $M \gg \sqrt{(2)}/p$ for adequate representation near $\theta = \pi$. For $p = 0.05$ this translates to $M \gg 28$. Furthermore, the integrand is zero at $\theta = \pi$, which suggests the need for M to be even for case 2. It will be shown that the largest contribution to the error for cases 2 and 3 comes from the segments aligned with the control points. These begin or end at $\theta = (2l - 1)\pi$ for any positive integer l.

Expression (5.7) of Ref. 12 gives the binormal velocity U_b normalized by $\Gamma/(4\pi R)$, where Γ is the circulation (as are all velocities

Received 20 May 2001; revision received 28 August 2001; accepted for publication 10 September 2001.

*Associate Professor, Department of Mechanical Engineering.
†Research Assistant, Department of Mechanical Engineering.

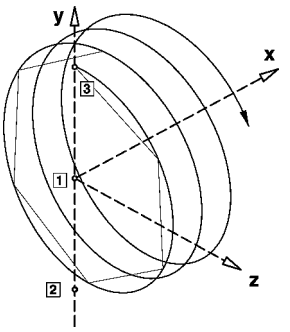

Fig. 1 Representation of helical vortex by straight segments.

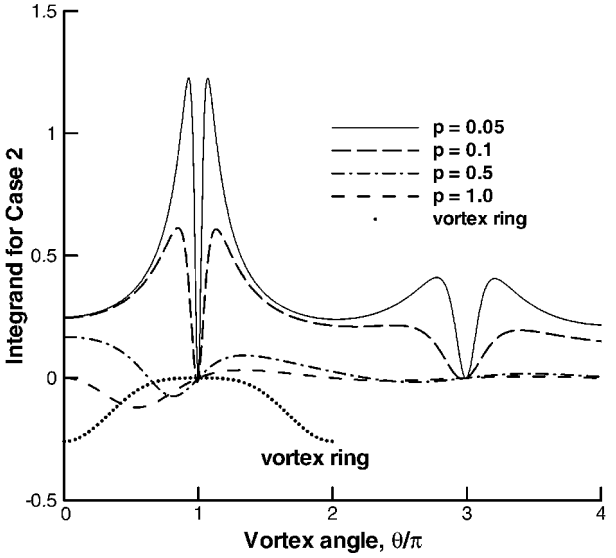

Fig. 2 Integrand in Eq. (1) for case 2.

in this paper), for any one of N identical vortices. Rearrangement gives

$$U_b = (p^2+1)^{\frac{1}{2}} \sum_{j=1}^{N-1} \left[W\left(\frac{2\pi j}{N}, p\right) - \frac{2p}{(p^2+1)} \right] + (p^2+1)^{\frac{1}{2}} W(p) - \frac{2p}{(p^2+1)^{\frac{1}{2}}} + \frac{1}{(p^2+1)} \left[\log 2 + 2p^2 - \frac{1}{2}\log(p^2+1) \right] - \underline{\frac{1}{(p^2+1)}\left(\log\varepsilon + \frac{1}{4}\right)} \qquad (1)$$

where the summed terms are caused by the other $N-1$ vortices and the remaining terms are the self-induced contribution. The integral $W(\alpha, p)$ is defined by Eq. (2.10) of Ref. 12 and $W(p)$ by Eq. (4.1) of Ref. 11. The last two underlined terms are the curvature terms, where $\varepsilon = a/(1+p^2)$. They arise from the Moore–Saffman procedure of treating the singularity in the Biot–Savart law for any curved vortex by subtracting the effects of the osculating circular vortex, whose velocity is well known (see Saffman[14]). The osculating vortex used in deriving Eq. (1) has a circular core containing evenly distributed vorticity. Ricca[9] discusses in detail the application of the Moore–Saffman procedure for helical vortices. Reference 11 shows that the final term $\frac{1}{4}$ would become zero if the vortex were a line vortex, whereas the logarithmic term would be unaltered. Thus we can anticipate that the structure of the core of a helical vortex contributes to its binormal velocity an amount of order $\frac{1}{4}$ at small pitch.

Neither $W(p)$ nor $W(\alpha, p)$ have, apparently, an analytic solution. Their asymptotic behavior was analyzed by Refs. 11 and 12, respectively. The latter show that, from Eq. (1), $U_b \to N/p$ as $p \downarrow 0$ for any $N \geq 1$, showing again that the limiting case of a helix at small pitch is not a vortex ring. If we take representative values of $p = 0.05$ and $\varepsilon = 0.032$ from Ref. 13, then $N/p \geq 20$ and $\log\varepsilon = -3.4$, so that the curvature term, which dominates the self-induced velocity of a vortex ring, is of secondary importance to a helix of sufficiently small pitch, as might be expected from a comparison of the integrands in Fig. 2. Furthermore, the curvature term tends to be cancelled by the higher-order pitch terms. It is clear, therefore, that there are sufficient differences between the motion of vortex rings and helices of small pitch to require the use of the latter in assessing the accuracy of the straight segment approximation. That is the aim of this work. The three test cases are described in more detail in the next section. This is followed by the results of the comparison and the conclusions.

Test Cases

Figure 1 shows the three test cases for a singly infinite helix of constant p and R beginning at $(x, y, z) = (0, 1, 0)$. In practice, this means that the blade shedding the helical tip vortex lies along the positive y axis ending at $(0, 1, 0)$. The coordinates of the control point for the first case are $(x_p, y_p, z_p) = (0, 0, 0)$. It is the only case with an exact solution $U = p^{-1}$, which is easily obtainable from the Biot–Savart law. This allows, for control points well away from the helix, the determination of the order of the straight segment approximation, which is not equivalent to any simple quadrature scheme on the original Biot–Savart integral. For case 1 the integrand decreases monotonically with θ or x.

The coordinates for case 2 $(x_p, y_p, z_p) = (0, -1, 0)$ would correspond to the tip of a second blade of a two- or four-bladed rotor or turbine. This gives rise to the essential difficulty shown in Fig. 2 without the complication of the curvature singularity for the self-induced velocity in case 3. Furthermore, cases 2 and 3 are well suited for comparison with the results of Ref. 12 who analyzed doubly infinite vortices, that is, vortices that also extend infinitely in the negative x direction. For cases 2 and 3 we calculate the binormal velocity U_b. The Biot–Savart law for case 2 can be written as

$$U_b = \frac{1}{(p^2+1)^{\frac{1}{2}}} \int_0^\infty \frac{-p^2\theta\sin\theta + (1-p^2)(1+\cos\theta)}{[p^2\theta^2 + 2(1+\cos\theta)]^{\frac{3}{2}}}\, \mathrm{d}\theta = \frac{(p^2+1)^{\frac{1}{2}} W(\pi, p)}{2} - p(p^2+1)^{-\frac{1}{2}} \qquad (2)$$

from Eq. (1) when $N = 2$ and considering the contribution from $j = 1$. (Alternatively, if $N = 4$, $j = 2$.) The integrand is shown in Fig. 2 for a range of p, and the values of $W(\pi, p)$ in Table 1 are taken from Table 1 of Ref. 12, which also gives $W(p)$. These values were obtained numerically and were checked by Refs. 11 and 12 against the asymptotic expansions of $W(p)$ and $W(\alpha, p)$ for small (and large) p. At $p = 0.05$ the numerical results agreed with the asymptotic expansion to the six significant figures shown in Table 1. Because the numerical quadrature should increase in difficulty as $p \downarrow 0$ (Fig. 2), it follows that the numerical results in Table 1 are accurate to six significant figures for all values of p. Based on the error analyses in Refs. 11 and 12 for the numerical calculations, the agreement with the asymptotic expansions has been extended to at least 10 significant figures for $W(p)$ and $W(\alpha, p)$ at $p = 0.05$. This work has not been reported; six significant figures are used here for consistency with Refs. 11 and 12. Furthermore, six figures corresponds to single precision on most computers and is easily sufficient to allow the main conclusions to be drawn.

Table 1 $W(\pi, p)$ and $W(p)$ to six significant figures

Pitch p	$W(\pi, p)$	$W(p)$	U_b for case 2	U_b for case 3
0.01	99.3069	95.7022	49.6459	48.1901
0.05	19.3086	17.3173	9.61642	8.96711
0.1	9.31407	8.01822	4.58076	4.28018
0.5	1.53777	1.34138	0.412426	0.735271
1.0	0.790427	0.456367	−0.148190	0.202238
5.0	0.190702	0.0711198	−0.494384	−0.0189082

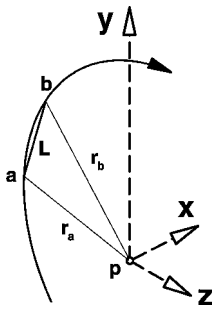

Fig. 3 Notation for Eq. (4) with the control point for case 1. The vortex segment begins at *a*, ends at *b*, and has length *L*.

For case 3 $(x_p, y_p, z_p) = (0, 1, 0)$, which is the start of the vortex. The Biot–Savart law gives

$$U_b = \frac{1}{(p^2+1)^{\frac{1}{2}}} \int_{\varepsilon}^{\infty} \frac{p^2\theta \sin\theta + (1-p^2)(1-\cos\theta)}{[p^2\theta^2 + 2(1-\cos\theta)]^{\frac{3}{2}}} \, d\theta$$

$$= \frac{(p^2+1)^{\frac{1}{2}} W(p)}{2} - \frac{p}{(p^2+1)^{\frac{1}{2}}} + \frac{1}{2(p^2+1)}$$

$$\times \left[\log 2 + 2p^2 - \frac{1}{2}\log(p^2+1) \right]$$

$$+ \frac{1}{2(p^2+1)} \left(\log\varepsilon + \frac{1}{4} \right) \tag{3}$$

from Eq. (1). The change in the lower limit of the Biot–Savart integral from zero to ε embodies the cutoff method, which Saffman[14] shows to be equivalent to the Moore–Saffman procedure for force-free vortices of the same core structure. $W(p)$ is given in Table 1. U_b is related to the x- and z-direction velocities U and W by

$$U_b = \frac{U \pm pW}{(p^2+1)^{\frac{1}{2}}} \tag{4}$$

where pW is added for case 2 and subtracted for case 3. For the straight-segment approximation U and W were found as the sum of the contribution from each segment U_s and W_s, for which the formulas are

$$\begin{bmatrix} U_s \\ W_s \end{bmatrix} = 2\frac{r_a + r_b}{r_a r_b \left[(r_a + r_b)^2 - L^2 \right]}$$

$$\times \begin{bmatrix} (y_p - y_b)(z_b - z_a) - (z_p - z_b)(y_b - y_a) \\ (x_p - x_b)(y_b - y_a) - (y_p - y_b)(x_b - x_a) \end{bmatrix} \tag{5}$$

as given by Eq. (2) of Afjeh and Keith.[1] The subscripts a and b denote the beginning and end of each segment and the lengths r_a, r_b, and L are defined in Fig. 3. All of the calculations were to 16 significant figures (double precision). The segments finished at a value of x determined as described in Section 4 of Ref. 11, and the remaining contribution to the infinite integral, the so-called "analytic remainder," was approximated by the first method of Wood and Meyer.[15] In no case did the analytic remainder contribute significantly to the integral.

Results

Figure 4 shows the errors for case 1 as a function of p and M. The error is the difference between the sum of the contributions from the vortex segments plus the analytic remainder and the exact result. For convenience, Figs. 4–6 show the absolute value of the error. It can be shown that the error for the first vortex segment [beginning at (0, 1, 0)] is approximately $2\pi^3/(3M^3)$, and the calculations agree with this value. As θ increases, the error changes sign and becomes dependent on M^{-2}, which presumably leads to the general M^{-2} dependence of the (positive) global error shown in Fig. 4. This dependence was also found by Refs. 2, 5, and 6 in their vortex ring comparisons.

The error for case 2 for small pitch, shown in Fig. 5a, is quite different from that in Fig. 4, even taking into account the six-figure accuracy of Table 1, which means, for example, that the large-M results for $p = 0.05$ and 0.1 cannot be trusted. For all values of p,

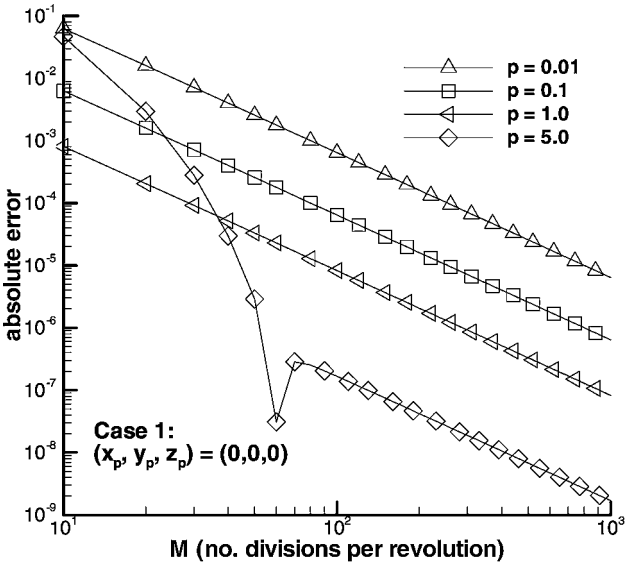

Fig. 4 Absolute error for case 1.

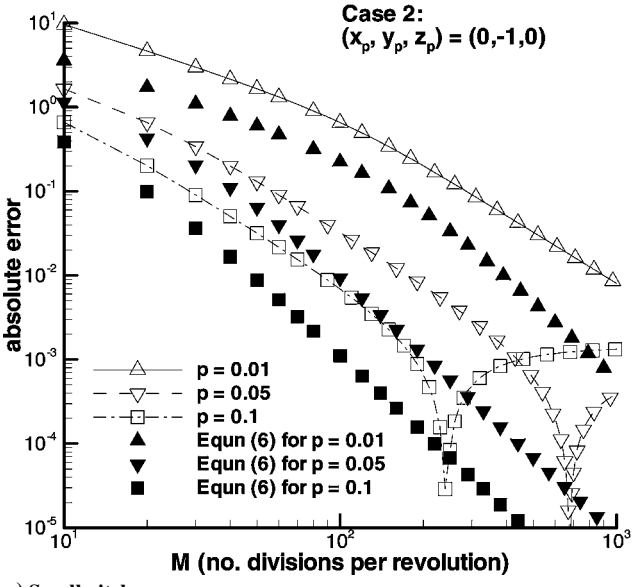

a) Small pitch

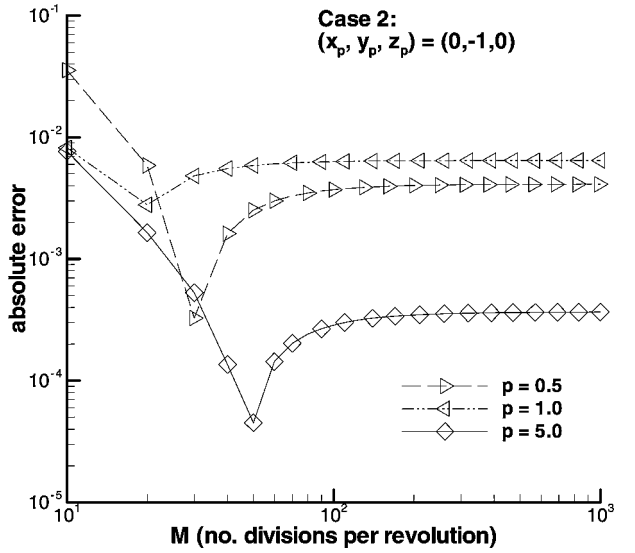

b) Large pitch

Fig. 5 Absolute error for case 2.

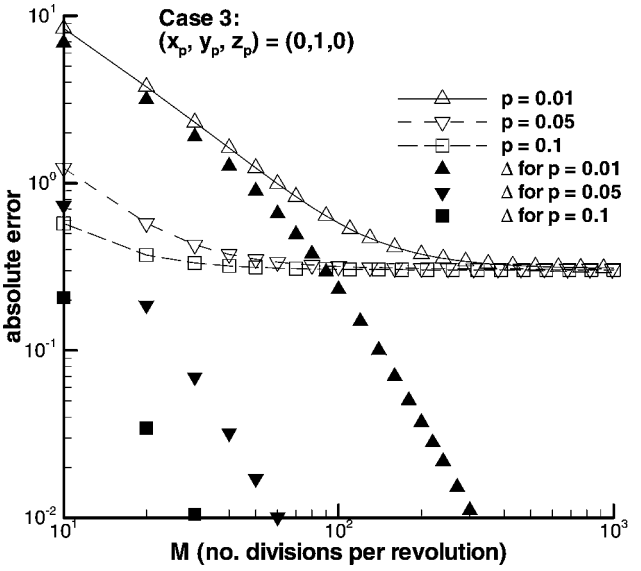

a) Small pitch

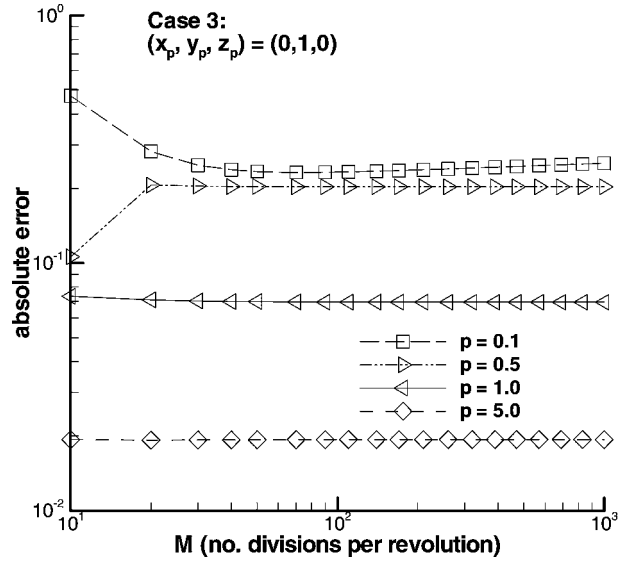

b) Large pitch

Fig. 6 Absolute error for case 3.

the errors before the minimum absolute error are negative, and all those afterward are positive.

At small p the error can be estimated from the following simple analysis. All vortex segments aligned with the control point have either y_a or $y_b = -1$ and give $U_s = 0$ by Eq. (5). This is because the velocity induced at a point by a straight vortex segment is normal to the plane containing the point and the segment. W_s is more difficult to analyze, but W_s for the segment ending at $(2l-1)\pi$, where l is a positive integer, tends to cancel that for the segment immediately following. (The cancellation is exact when $p = 0$.) Furthermore, W_s is multiplied by p in Eq. (4), so that it can be assumed that the contribution to the binormal velocity is zero from the aligned segments. Now the integrand in Eq. (2) is zero if $\theta = (2l-1)\pi$ for any positive integer l, so we can use the trapezoidal rule to estimate the error caused by the zero contribution from the two aligned segments for each l. To the accuracy of the trapezoidal rule, this error does not depend on the $\sin\theta$ term in Eq. (2). The approximate error is

$$-\tfrac{1}{2}(1+p^2)^{\frac{1}{2}}(2\pi/M)^3\{[(2l-1)\pi p]^2 + (2\pi/M)^2\}^{-\frac{3}{2}}$$

Summing over all l, and then approximating the sum by an integral, gives the global error Δ as

$$\Delta \approx -\frac{(1+p^2)^{\frac{1}{2}}}{2pM}\left\{1 - \frac{p(M/2+1)}{[(pM/2)^2 + p^2M + p^2 + 1]^{\frac{1}{2}}} + \frac{1}{2[(pM/2)^2 + p^2M + p^2 + 1]^{\frac{3}{2}}}\right\} \tag{6}$$

The absolute value of Eq. (6) is shown in Fig. 5a for the three lowest p. Equation (6) underestimates the error by a factor of about two, but the sign and trend of the actual error with increasing M are accurately reflected by the simple formula. The straight segment approximation is, therefore, only first-order accurate at small M, approximately $M < 30$ for $p = 0.05$, improving to third order at much larger M. Neither of these results is obtainable from comparison with the velocity field of a vortex ring. Because the error appears to be dominated by the aligned segments, it follows that the test cases involving a helix of constant diameter and pitch are likely to be the severest possible. It can be shown empirically that the ratio of the actual error to Δ scales on the product pM at small pitch, at least until $pM \approx 5$. The analysis leading to Eq. (6) is only valid at small p, and so it is not surprising that the form of the error changes markedly as p increases (Fig. 5b).

Figure 6 shows the results for case 3, for which the Biot–Savart integrand in Eq. (3) behaves as θ^{-1} as $\theta \to 0$, giving rise to the logarithmic curvature singularity. However, $U_s = W_s = 0$ for the first segment, as a straight vortex cannot induce any velocity on itself. This suggests that the underlined curvature terms in Eq. (3) should be excluded from the determination of the error; they were excluded in preparing Fig. 6. An approximate correction for the first segment error can be found by integrating the leading term in Eq. (3) as $\theta \to 0$, $[2(1+p^2)\theta]^{-1}$, from $\theta = \varepsilon$ to $\theta = 2\pi/M$, the end of the first segment. For small p the relative error in approximating the integrand by the leading term is $\pi^2/(2M^2)$, which is less than 0.008 for $M > 25$. Integration yields $\log(2\pi/M)/2(1+p^2) - \log\varepsilon/2(1+p^2)$; the latter cancels the first underlined term in Eq. (3). $\log(2\pi/M)/2(1+p^2)$ was added to the binormal velocity calculated from Eqs. (4) and (5). U_s from the second segment was found to be within 10% of the Biot–Savart value at small pitch, and so its error was not analyzed. It is clear from Fig. 6a that this procedure for dealing with the curvature singularity is simple and successful. Bhagwat and Leishman[6] reached a similar conclusion from their vortex ring comparisons.

The remaining vortex segments aligned with the control point play a similar role as they did in case 2: there is no significant contribution to U_b from any segment, which has either y_a or $y_b = 1$. A straightforward extension of the preceding analysis (excluding the first segment!) shows Δ for case 3 to be that given by Eq. (6) with $M/2$ in the square brackets replaced by M. This expression for Δ is applicable for small p, Fig. 6a, suggesting that the aligned segments dominate the error for case 3, as they did for case 2. This leads to the same estimate for the order of the vortex segment approximation at small M. At large M, however, the error tends to a constant: nearly 0.30 for the three smallest values of p. This has the same magnitude as the second underlined term in Eq. (3) due to the internal structure of the vortex, which is only known in any detail for the wake of hovering rotors, e.g., Ref. 13. On these grounds it is premature to aim for accuracy greater than that achievable from adding $\log(2\pi/M)/2(1+p^2)$ to the binormal velocity calculated from straight-segment equations (5). It is worth noting, however, that it is necessary to have $M > 80$ to achieve an error of 0.30 at $p = 0.05$. This value of M is larger than that used in many calculations. As the pitch increases (Fig. 6b), the form of the error changes significantly, for reasons similar to those advanced for case 2.

Conclusions

This paper discusses the accuracy of representing a helical vortex by straight segments when determining the induced velocity. For the first time the accuracy of this approximation was tested for a semi-infinite vortex of constant pitch and radius rather than a vortex ring as has been used in numerous previous studies. It is shown that a vortex ring is not a special case of a helix as the pitch decreases and that several important aspects of the straight segment approximation

are only available from the comparison with a helix. Three test cases were considered over a wide range of the vortex pitch. Attention was concentrated on the errors at the small values of the pitch typical of wind turbine and hovering rotor wakes.

The control point for case 1 was on the centerline of the start at the vortex. Comparison to the exact solution showed the accuracy of the straight segment representation for control points well away from the helix to be second order in, say, the number of vortex segments per revolution of the helix M. The straight segment approximation is thus of the same order as the trapezoidal rule applied to the original Biot–Savart integral.

The other two cases do not have exact solutions, and so recourse was made to the recent, very accurate numerical results of Refs. 11 and 12 for the velocity of the vortex itself and for points at the same radius as the vortex. These results were verified by comparison to asymptotic expansions for small and large pitch. The control point in the second case is displaced 180 deg from the vortex, and the third case considered the self-induced velocity. In both these cases attention was drawn to those vortex segments aligned with the control point, as they do not contribute to the velocity. Such alignment can also occur with vortex rings, but there can be at most two aligned segments for a ring, whereas there are infinitely many for the helices in cases 2 and 3. Furthermore, as demonstrated in Fig. 2, the integrand for the Biot–Savart integral is considerably smaller for vortex rings than helices of small pitch. This observation points to the necessity of using helical vortices rather than vortex rings to assess the accuracy of the straight segment approximation. Second, it suggests that the present test cases are more severe than, say, a vortex that is expanding or contracting. Third, it leads to a very simple error analysis that is surprisingly useful in determining the form of the error. Equation (6) indicates that the error for both cases 2 and 3 at small pitch is first order for small M, rising to third order at large M. For small pitch the value of M to minimize the error is much larger than used in most calculations.

The curvature singularity for the self-induced velocity case 3 was easily dealt with, as has been shown earlier for a vortex ring.[6] With a simple correction for the first straight segment (attached to the control point), the error tends to a constant at large M and small pitch. The magnitude of this constant is comparable to the contribution to the self-induced velocity that arises from the internal structure of the vortex core. It would be premature to attempt to improve upon the accuracy shown in Fig. 6a until more information is available on the internal structure of tip vortices. As the pitch increases, the error for the self-induced velocity behaves similarly to that in case 2.

Acknowledgment

This work was funded by the Australian Research Council.

References

[1]Afjeh, A. A., and Keith, T. G., "A Simplified Free Wake Method for Horizontal-Axis Wind Turbine Performance Prediction," *Journal of Fluids Engineering*, Vol. 108, No. 4, 1986, pp. 400–406.

[2]Bliss, D. B., Teske, M. E., and Quackenbush, T. R., "A New Methodology for Free Wake Analysis Using Curved Vortex Segments," NASA CR 3958, 1987.

[3]Xu, G., and Sankar, L. N., "Computational Study of Horizontal Axis Wind Turbines," *Journal of Solar Energy Engineering*, Vol. 122, No. 1, 2000, pp. 35–39.

[4]Bhagwat, M. J., and Leishman, J. G., "Stability Analysis of Helicopter Rotor Wakes in Axial Flight," *Journal of the American Helicopter Society*, Vol. 45, No. 3, 2000, pp. 165–178.

[5]Bhagwat, M. J., and Leishman, J. G., "Stability, Consistency and Convergence of Time-Marching Free-Vortex Rotor Wake Algorithms," *Journal of the American Helicopter Society*, Vol. 46, No. 1, 2001, pp. 59–70.

[6]Bhagwat, M. J., and Leishman, J. G., "Accuracy of Straight-Line Segmentation Applied to Curvilinear Vortex Filaments," *Journal of the American Helicopter Society*, Vol. 46, No. 2, 2001, pp. 166–169.

[7]Gupta, B. P., and Loewy, R. G., "Theoretical Analysis of the Aerodynamic Stability of Multiple, Interdigitated Helical Vortices," *AIAA Journal*, Vol. 12, No. 10, 1974, pp. 1381–1387.

[8]Hardin, J. C., "The Velocity Field Induced by a Helical Vortex Filament," *Physics of Fluids*, Vol. 25, No. 11, 1982, pp. 1949–1952.

[9]Ricca, R. L., "The Effect of Torsion on the Motion of a Helical Vortex Filament," *Journal of Fluid Mechanics*, Vol. 273, 1994, pp. 241–259.

[10]Kuibin, P. A., and Okulov, V. L., "Self-Induced Motion and Asymptotic Expansion of the Velocity Field in the Vicinity of a Helical Vortex Filament," *Physics of Fluids*, Vol. 10, No. 3, 1998, pp. 607–614.

[11]Boersma, J., and Wood, D. H., "On the Self-Induced Motion of a Helical Vortex," *Journal of Fluid Mechanics*, Vol. 384, 1999, pp. 263–280.

[12]Wood, D. H., and Boersma, J., "On the Motion of Multiple Helical Vortices," *Journal of Fluid Mechanics*, Vol. 449, 2001, pp. 149–171.

[13]Leishman, J. G., Baker, A., and Coyne, A., "Measurements of Rotor Tip Vortices Using Three-Component Laser-Doppler Velocimetry," *Journal of the American Helicopter Society*, Vol. 41, Oct. 1996, pp. 342–353.

[14]Saffman, P. G., *Vortex Dynamics*, Cambridge Univ. Press, New York, 1992, Chap. 11.

[15]Wood, D. H., and Meyer, C., "Two Methods for Calculating the Velocities Induced by a Constant Diameter Far-Wake," *Journal of Aircraft*, Vol. 28, No. 8, 1991, pp. 526–531.

A. Plotkin
Associate Editor